Adaptive-robust friction compensation in a hybrid brake-by-wire actuator

Ricardo de Castro[1], Fabio Todeschini[2], Rui E Araújo[3,4], Sergio M Savaresi[2], Matteo Corno[2] and Diamantino Freitas[3]

Date received: 2 April 2013; accepted: 3 September 2013

Introduction

With the progressive increase in the safety, comfort, and performance requirements of modern vehicles, the automotive industry is considering brake-by-wire (BBW) approaches as an attractive option to replace the hydraulic-based brake systems. For example, in contrast to the traditional brake systems based on solenoid valves that only admit discrete control actions (e.g. increase, hold, decrease), BBW actuators allow an accurate and continuous action over the braking torque. This feature, together with the higher bandwidths provided by the BBW, is a great asset for (1) improving the effectiveness of braking assistance functionalities, like anti-lock braking systems;[1,2] (2) providing better actuation capabilities for the vehicles' lateral safety systems that may depend on differential braking;[3] and (3) facilitating the torque blending between friction brakes and regenerative torque available in electric vehicles.[4] Another significant feature of the BBW system is the elimination of the mechanical link between the brake pedal and the wheel brakes. This isolation is beneficial from a comfort perspective because it enables the implementation of haptic pedal feedback with custom brake feel. On the contrary, it also introduces major challenges to ensuring fail-safe operation.[5]

Generally, there are two main options for the BBW implementation: electro-hydraulic braking (EHB)[6,7] and electro-mechanical braking (EMB).[8,9] The main attractiveness of the former option is the possibility of maintaining a significant portion of the components used in the braking system of today's vehicles, such as calipers, hydraulic link, and accumulators.[6,7,10] Given

[1]Institute of System Dynamics and Control, Robotics and Mechatronics Center, German Aerospace Center (DLR), Wessling, Germany
[2]Dipartimento di Elettronica, Informazione e Bioingegneria, Politecnico di Milano, Milano, Italy
[3]Department of Electrical and Computer Engineering, Faculdade de Engenharia da Universidade do Porto, Porto, Portugal
[4]INESC TEC (formerly INESC Porto), Porto, Portugal

Corresponding author:
Ricardo de Castro, Institute of System Dynamics and Control, Robotics and Mechatronics Center, German Aerospace Center (DLR), Wessling D-82234, Germany.
Email: Ricardo.DeCastro@dlr.de

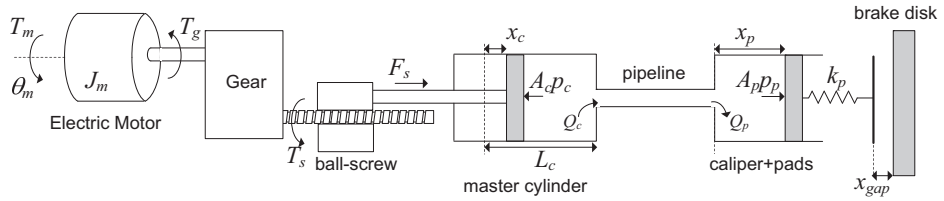

Figure 1. Block diagram of the BBW actuator.

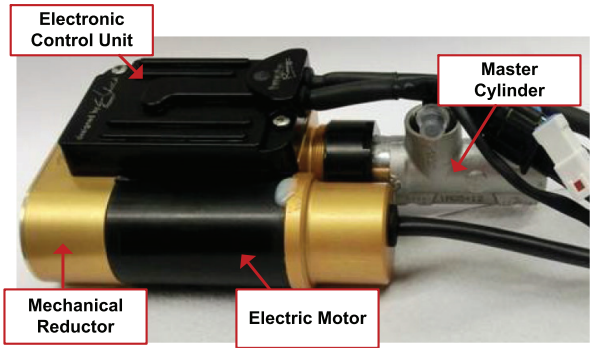

Figure 2. Brake-by-wire prototype.

that most of these components have already reached a mature state of development, this normally brings cost and reliability advantages to the EHB solution. The second option, EMB, relies on a pure mechanical link between the actuator and the brake disc. Compared with the EHB, it allows a significant decrease in the volume, weight, and component number, and also offers faster response times.[9,11] However, the EMB requires a major redesign of today's braking systems, and while such actuators do not reach a mass-production stage, the cost will remain an issue. Therefore, this factor, together with the fail-safe concerns, still represents a significant obstacle for the widespread use of pure EMB designs.

Spurred by these challenges, the automotive industry in recent years has dedicated considerable efforts towards improving EHB and EMB designs. In this work, we explore an emerging BBW prototype, under development by an Italian brake manufacturer, which intends to hybridize the EHB and EMB approaches. The main idea behind this hybrid BBW, illustrated in Figures 1 and 2, is, just like the EHB, to keep intact the calipers and the braking lines of today's vehicles. However, instead of using electro-valves, accumulators, and pumps to regulate the braking pressure (as is done in EHB), an electro-mechanical actuator, that is, an electric motor–gear–ball-screw, is directly connected to the piston of the master cylinder to generate the braking pressure. With this approach, the cost and the number of components can be kept relatively low, as we only need to fit one additional element, the electro-mechanical actuator, in the braking system. This latter feature is also very beneficial for vehicles subject to strong space constraints, for example, motorbikes.[12,13] Furthermore, given the high bandwidth of the electro-mechanical actuator, the response times of the hybrid configuration are expected to be faster than the ones obtained with the EHB (but slower than the pure EMB, due to the hydraulic link).

In this context, the main goal of this work is to develop an electronic controller for the above-mentioned hybrid BBW, capable of robustly regulating the braking force. In the literature, there are several studies on the design of braking (or clamping) force control for pure EMB designs, ranging from linear proportional–integral–derivative (PID) techniques,[14] force–speed cascaded loops,[15] model predictive controllers,[9] or robust time-optimal approaches.[16] Despite being useful for pure EMB actuators, the controllers' designs presented in these studies cannot be directly applied to the hybrid BBW configuration under study here. This is due to the existence of the hydraulic link in the actuator, which introduces non-negligible dynamics that must be taken into account at the controller's design stage. To overcome this limitation, in this work, we propose a practical controller for the hybrid BBW actuator that considers these non-negligible dynamics.

Besides the hydraulic link, friction represents another major source of disturbance in the BBW actuator, which may lead to the appearance of limit cycles, stick-slip, and steady-state tracking errors. From a control perspective, several approaches can be used to mitigate the friction effects, such as dither, position-error dead band, and model-based compensation techniques.[17] Among these techniques, the model-based compensation, that is, incorporation in the controller of a feedforward component to cancel the friction disturbance,[17] has emerged in recent years as the most promising technique. One of the main reasons for this interest lies in the possibility to combine model-based friction compensation with adaptive control methods. This enables the controller to handle, online, parameter changes in the friction disturbance (which may appear as a result of variations in temperature, wear, etc.). Since the friction model is generally non-linear, particularly the Stribeck effect, the construction of the adaptation laws is also greatly simplified if the (friction) disturbance can be represented with a

linear-in-the-parameter (LP) structure,[18] that is, linear in the unknown parameters. The recent literature contains several works that approximate the non-linear friction map with LPs based on linearization techniques,[19,20] polynomials,[21,22] Lorentzian,[17,23] and piecewise linear functions.[24–26] Most of these approaches, however, assume an accurate knowledge of the so-called Stribeck velocity, a parameter that characterizes the transition speed between the static and kinetic (Coulomb) friction regimes. In practice, due to parametric variation resulting from various factors (temperature, humidity, etc.), this assumption does not always hold.

An additional contribution of this work is to offer a new LP, composed of a sum of normalized exponentials, capable of approximating the non-linear friction map with a significant uncertainty in the Stribeck velocity. This new LP, obtained through optimal function approximation techniques, provides a higher accuracy than the LPs previously proposed in the literature[19–21,26] and has a reduced number of basis functions (six). In the second part of this work, the optimal LP is employed in the development of an adaptive-robust controller for the hybrid BBW actuator. It is shown that, under some reasonable assumptions, the actuator can be modelled as an uncertain second-order system, affected by two types of disturbances: parametric and non-parametric. The former, arising from the approximation of friction with an LP, is compensated using a switching-σ adaptation mechanism. The latter, resulting from modelling approximations, is attenuated with a continuous sliding mode term. The robust stability and ultimate boundedness of the proposed controller are established analytically through the Lyapunov method. A preliminary version of this work was presented in the Mechatronics 2012 conference[27] and is extended here with additional discussion on the (reduced) model of the BBW and experimental validation of the control law.

Actuator model

As shown in Figure 1, the BBW actuator under consideration is composed of different types of physical sub-systems, involving electrical, mechanical, and hydraulic domains. The main source of motion lies in the electric motor (direct current (DC) motor, with 200 W), which is connected to a fixed reduction gear to increase the output torque. This rotational motion is then converted in linear displacement, for example, by using a ball-screw device, pushing the master cylinder piston, and building up the necessary braking pressure. The hydraulic pressure is conducted through a small pipeline (i.e. the brake lines) to the pads, which then presses the braking disc to generate the clamping force.

Mathematical model

Starting with the electro-mechanical part of the actuator, we have

$$J_m\ddot{\theta}_m = T_m - T_g - T_f(.) \tag{1a}$$

$$m_c\ddot{x}_c = F_s - p_cA_c \tag{1b}$$

$$T_g = \frac{F_s}{G},\ \theta_m = Gx_c \tag{1c}$$

$$\tau_m\dot{i}_m = -i_m + i_m^*,\ T_m = k_mi_m \tag{1d}$$

The first equation represents the rotational dynamics of the motor, where θ_m is the motor position, J_m is the sum of motor and reduction gear inertias, T_m is the torque generated by the electric motor, T_g is the torque at the gearbox input, and T_f is the equivalent friction torque. To simplify the model, it is presumed that the main friction forces that affect the actuator (e.g. the friction in reduction gear, ball-screw, piston, pipeline) can be referred to the electric motor side; we postpone the mathematical definition of T_f to a later section. The second equation models the linear displacement of the cylinder, with m_c representing the piston mass, x_c representing the position, F_s representing the linear force applied by the ball-screw, p_c representing the master cylinder pressure, and A_c representing its area. The third equation describes the relation between torque/force and rotation/linear position present in the reduction gear and ball-screw mechanisms, having G (rad/m) as the overall gain factor. Finally, equation (1d) represents the closed-loop response of the motor current controller, where i_m is the motor current, i_m^* is the set-point, τ_m is the dominant time constant, and k_m (Nm/A) is the current/torque gain. For the sake of brevity, this work omits the details regarding the design of the inner current loop (the interested reader is referred to Dardanelli et al.[12] and Acquistapace and Mazzoleni[28] for additional information on this inner loop).

After specifying the electro-mechanical model, we move on to the modelling of the hydraulic section. Following similar arguments as those exposed in Dardanelli et al.,[12] the pressure dynamics in the master and pad cylinders can be established by the direct application of the continuity equation[29]

$$-Q_c = \dot{V}_c + \frac{V_c}{\beta}\dot{p}_c \tag{2a}$$

$$Q_p = \dot{V}_p + \frac{V_p}{\beta}\dot{p}_p \tag{2b}$$

$$V_c = (L_c - x_c)A_c,\ V_p = A_px_p \tag{2c}$$

where Q_c is the volumetric flow rate getting out of the master cylinder chamber; Q_p is the volumetric flow entering the pad's cylinder; V_c and V_p are the volume of the master and pad cylinders, respectively; A_p is the area of the pad cylinder piston, and β is the bulk modulus of the brake fluid. Neglecting the pipeline dynamics,

Table 1. Physical parameters of the BBW actuator.

Variable	Symbol	Value
Inertia of motor + gear	J_m	1.1×10^{-5} kg m^2
Mass of the master cylinder piston	m_c	1×10^{-2} kg
Combined reduction ratio	G	3.294×10^{3} rad/m
Time constant of the current loop	τ_m	15.9×10^{-3} s
Current/torque gain	k_m	16.8×10^{-3} Nm/A
Area of the master cylinder	A_c	1.13×10^{-4} m^2
Length of the master cylinder	L_c	29×10^{-3} m
Bulk modulus of the brake fluid[a]	β	1.6×10^{9} Pa
Area of the pad's cylinder	A_p	3.22×10^{-3} m^2
Stiffness of the pad[a]	k_p	1.28×10^{8} N/m
Pipeline width	–	8×10^{-3} m
Pipeline length	–	0.8 m

[a]Nominal value.

and assuming laminar flow, we can further derive the pressure decrease in the pipeline as

$$p_c - p_p = K_{cp}Q, \quad Q = Q_c = Q_p \tag{3}$$

where K_{cp} is the laminar flow coefficient of the pipeline (which depends on the conduct geometry and fluid properties).[29] Finally, the clamping force applied to the brake disc can be described by the following dynamic model

$$m_p\ddot{x}_p = p_pA_p - F_c(x_p) \tag{4a}$$

$$F_c(x_p) = \begin{cases} 0, & \text{if } x_p < x_{gap} \\ k_p(x_p - x_{gap}), & \text{if } x_p \geqslant x_{gap} \end{cases} \tag{4b}$$

where m_p is the pad mass, x_p is the pad displacement, x_{gap} is the air gap between the brake disc and the pad, k_p is the stiffness of the pad, and F_c is the clamping force. Table 1 contains a list of the known values of some of the physical parameters of the actuator.

Development of a control-oriented model

This section aims to develop a practical mathematical model that can be helpful in the design of feedback controllers for the BBW actuator. To clarify the role of the numerous variables introduced in the previous section (i.e. define states, parameters, disturbances, etc.), it is convenient to first rewrite the system models (1)–(4) in a state space formulation. Accordingly, let us consider the following state variables

$$x_1 = \theta_m,\ x_2 = \dot{\theta}_m = \omega_m,\ x_3 = p_c \tag{5a}$$

$$x_4 = p_p,\ x_5 = x_p,\ x_6 = \dot{x}_p,\ x_7 = i_m \tag{5b}$$

$$\mathbf{x} = \begin{bmatrix} x_1 & x_2 & x_3 & x_4 & x_5 & x_6 & x_7 \end{bmatrix}^T \tag{5c}$$

By replacing these variables in equations (1)–(4), and considering the motor current setpoint as the control input for the system, that is, $u = i_m^*$, the system dynamics is given as

$$\dot{x}_1 = x_2 \tag{6a}$$

$$J_{eq}\dot{x}_2 = k_m x_7 - \frac{A_c}{G}x_3 - T_f(.) \tag{6b}$$

$$\dot{x}_3 = \frac{\beta}{L_c - \frac{x_1}{G}A_c}\left(\frac{A_c}{G}x_2 - \frac{x_3 - x_4}{K_{cp}}\right) \tag{6c}$$

$$\dot{x}_4 = \frac{\beta}{A_p x_5}\left(\frac{x_3 - x_4}{K_{cp}} - A_p x_6\right) \tag{6d}$$

$$\dot{x}_5 = x_6 \tag{6e}$$

$$m_p\dot{x}_6 = \left(x_4A_p - F_c(x_5)\right) \tag{6f}$$

$$\tau_m\dot{x}_7 = (-x_7 + u) \tag{6g}$$

where $J_{eq} = J_m + m_c/G^2$ is the equivalent inertia of the motor, gear, ball-screw, and mass of master cylinder's piston.

Before presenting the development of the reduced model, it is pertinent to discuss some of the possible control variables that can be used by the BBW controller. Ideally, the BBW controller should use the braking torque (or, alternatively, the clamping force F_c) as the controlled variable. However, due to the package and cost constraints, it is not always desirable/possible to have dedicated sensors to measure these variables. Therefore, in practice, it is more convenient to exert an indirect control over the braking torque using easily measurable variables, such as hydraulic pressure. In the BBW actuator employed in this work, and taking into account our goal of keeping intact the calipers used in today's vehicles, the variable that is more easily measurable and, simultaneously, has a strong connection with the braking torque is the pressure in the master cylinder, $x_3 = p_c$. Consequently, in the sequel, we will regard x_3 as the main output of the actuator's reduced model.

Simplification of the hydraulic and pad's model

Starting with the pad's model, it is noteworthy to verify that equation (6f) is a hybrid/switching system, in the sense that the model's vector field is dependent on the value of the binary condition

$$c_g = (x_5 \geqslant x_{gap}) \in \{0, 1\} \tag{7}$$

Generally, this condition will affect the control strategy employed in the actuator. For example, in situations where $c_g = 0$, an air gap management algorithm is normally used to overcome the clearance gap between the pads and the braking disc. This operation, seen as an initial procedure to prepare the actuator for the braking manoeuvre, can be achieved with the help of prefilling functionalities[30] or by controlling the pad's position.[13,14,16,31] On the contrary, after putting the pads in direct contact with the braking disc (i.e. $c_g = 1$), the

control goal is to track the (hydraulic brake) pressure setpoint. Throughout this work, the following assumption will be considered.

Assumption 1. The pads are always in direct contact with the braking disc, that is, $x_p = x_5 \geqslant x_{gap}$. Thus, the control-oriented model will be valid in the domain

$$\mathcal{X} = \{\mathbf{x} | x_5 \geq x_{gap}\} \tag{8}$$

This assumption can be ensured by employing a suitable gap clearance management every time the BBW controller is active, as mentioned above. Additionally, to further simplify equation 6(f), we will consider the following.

Assumption 2. After the pads encounter the braking disc, the inertial force of the pads ($m_p \dot{x}_6$) can be neglected.

This simplification allows us to find an (approximate) algebraic relation between the pad's pressure and position, as well as its time derivative

$$k_p(x_p - x_{gap}) \approx p_p A_p, \quad k_p \dot{x}_p \approx \dot{p}_p A_p, \quad \forall x_p \geqslant x_{gap} \tag{9}$$

By replacing the above relations in equations (6c)–(6f), the equations associated with the pad position (x_5) and speed (x_6) can be dropped, and the dynamics of the master cylinder pressure (x_3) and the pad's pressure (x_4) posed with the following representation

$$\dot{x}_3 = \Gamma(x_1)(x_2 - \alpha_1(x_3 - x_4)) \tag{10a}$$
$$\dot{x}_4 = \alpha_2 \Xi(x_4)(x_3 - x_4) \tag{10b}$$

$\mathbf{x} \in \mathcal{X}$, which depends on two parameters

$$\alpha_1 = \tfrac{G}{A_c K_{cp}}, \ \alpha_2 = \tfrac{k_p}{K_{cp} A_p^2} \tag{11}$$

and two non-linear functions

$$\Gamma(x_1) = \tfrac{\beta}{L_c G - x_1}, \ \Xi(x_4) = \left(1 + \tfrac{x_4 + x_{gap}\frac{k_p}{A_p}}{\beta}\right)^{-1}$$

Inspecting more closely the last function, $\Xi(x_4)$, one can find that the pad's pressure (x_4) and the bulk modulus of the braking fluid β are the most relevant variables in the function. Since, in practice, β takes very high values (see, for example, the nominal value of β presented in Table 1), we can use the following result.

Assumption 3. (high value of the bulk modulus).

$$\beta \gg x_4 + x_{gap}\frac{k_p}{A_p} \tag{12}$$

to approximate the function $\Xi(x_4)$ with a constant, unitary value that is $\Xi(x_4) \approx 1$. Consequently, equation (10) can be further simplified as

$$\dot{x}_3 = \Gamma(x_1)(x_2 - \alpha_1(x_3 - x_4)), \ \dot{x}_4 = \alpha_2(x_3 - x_4) \tag{13}$$

From these relations, it is worth emphasizing that the main driving forces behind x_3 dynamics are the motor speed (x_2) and the pressure difference $x_3 - x_4$ in the pipeline. Since this last quantity also plays an important role in the dynamics of the pad's pressure x_4, it seems reasonable to consider the pressure difference

$$\Delta_p = x_3 - x_4 \tag{14}$$

as an alternative state variable to x_4. In particular, by introducing Δ_p in equation (13), we obtain

$$\dot{x}_3 = \Gamma(x_1)(x_2 - \alpha_1 \Delta_p) \tag{15a}$$
$$\dot{\Delta}_p = \Gamma(x_1)x_2 - (\Gamma(x_1)\alpha_1 + \alpha_2)\Delta_p \tag{15b}$$

By joining these last two equations, the master cylinder dynamics can be expressed as

$$\dot{x}_3 = \frac{\alpha_2}{\alpha_1 + \frac{\alpha_2}{\Gamma(x_1)}} x_2 + \frac{\alpha_1}{\alpha_1 + \frac{\alpha_2}{\Gamma(x_1)}} \dot{\Delta}_p \tag{16a}$$
$$= \frac{\alpha_2}{\alpha_1} x_2 + \underbrace{\frac{1}{1 + \frac{\alpha_2}{\alpha_1 \Gamma(x_1)}} \left(\dot{\Delta}_p - \frac{\alpha_2^2}{\alpha_1^2 \Gamma(x_1)} x_2 \right)}_{\delta\left(x_1, x_2, \dot{\Delta}_p\right)} \tag{16b}$$
$$= \frac{\alpha_2}{\alpha_1} x_2 + \delta(x_1, x_2, \dot{\Delta}_p) \tag{16c}$$

Assumption 4. For control purposes, we will regard the term $\delta(x_1, x_2, \dot{\Delta}_p)$ as a bounded disturbance that the BBW controller should attenuate. It is also convenient to consider that this disturbance has a bounded time derivative, which means that, from now on, we will work under the premise that

$$|\delta(.)| \leqslant \bar{\delta}_0, \ |\dot{\delta}(.)| \leqslant \bar{\delta}_1, \ \forall \mathbf{x} \in \mathcal{X} \tag{17}$$

where $\bar{\delta}_0$ and $\bar{\delta}_1$ are upper bounds.

Assumption 5. In light of the fast response of the inner current loop, the dynamics of this loop will be neglected, thus $x_7 = i_m \approx i_m^* = u$.

Using these last assumptions, together with equations (16c) and (6b), the control-oriented model that we propose for the actuator is described by the following uncertain second-order system

$$J_{eq} \dot{x}_2 = k_m u - \frac{A_c}{G} x_3 - T_f(.) \tag{18a}$$
$$\dot{x}_3 = \frac{\alpha_2}{\alpha_1} x_2 + \delta(.) \tag{18b}$$

which is valid for $\mathbf{x} \in \mathcal{X}$. In comparison with equation (6), the above reduced representation, albeit less accurate, is a much more tractable model for control design purposes.

Validation of the reduced hydraulic model

The structure proposed in equation (18) is composed of two parts: (1) the x_2 dynamics, associated with the

electro-mechanical part, and (2) the x_3 dynamics, related to the hydraulic pressure in the master cylinder. With regard to the electro-mechanical part, and given that we did not make any special simplifications to equation (18a), this relation is expected to be sufficient to characterize the response of the motor speed. On the contrary, the cylinder's reduced model, equation (18b), was subjected to a series of strong simplifications in the hydraulic and pad dynamics, and there are legitimate concerns about the validity of such approximations. To dissipate such concerns, we will demonstrate, through experimental tests, that equation (18b) can capture the fundamental dynamics of the actuator, and that the assumptions employed in the model's derivation are valid.

Recall that equation (18b) builds on the hypothesis that the fundamental relation between the motor speed x_2 and the pressure x_3 is described by an integral relation (assuming the undisturbed situation $\delta \approx 0$)

$$\dot{x}_3 \approx \frac{\alpha_2}{\alpha_1} x_2, \; \mathbf{x} \in \mathcal{X} \tag{19}$$

To validate this hypothesis, it is helpful to regard the motor speed $x_2 = \omega_m$ as a 'pseudo-input' for the hydraulic model, while the pressure $x_3 = p_c$ is the output. Of course, in practice, the true control input for the BBW controller will be the motor current setpoint, and we will also have to take into consideration the motor dynamics, that is, equation (18a). Nonetheless, for validating the candidate model (19), it is much more interesting to decouple the hydraulics from the electro-mechanical part, as this latter sub-block is subject to difficult-to-model non-linearities, like friction (topic to be addressed in the next section), which brings unnecessary complications to the identification process.

Since equation (19) only depends on one parameter, that is, the ratio $\vartheta = \alpha_2/\alpha_1$, the identification process of this model is relatively straightforward. In fact, considering a continuous-time identification approach, the parameter ϑ can be estimated by solving the following least-squares problem

$$\min_{\hat{\vartheta}} \int_0^T \left(p_c(t) - \underbrace{\left(\hat{\vartheta} \int_0^t (\omega_m(\tau) d\tau + p_c(0)) \right)}_{\hat{p}_c(t)} \right)^2 dt \tag{20}$$

where T is the duration of the test, $\omega_m(t)$ is the measured motor speed (model input), $p_c(t)$ is the measured pressure in the master cylinder (model output), and $\hat{p}_c(t)$ is the estimated pressure. To experimentally validate the simplified hydraulic model, the BBW actuator was installed in a test bench, the details of which are provided in section 'Experimental validation'.

A pseudo-random binary signal was applied to the motor current, having a significant power spectrum up to 10 Hz (see Figure 3(a)), which represents the intended working range for the actuator. After collecting the measurements p_c and ω_m, the fitting problem (20) was discretized and then numerically solved, producing the estimative $\hat{\vartheta} = 2.99\, bar/rad$. As illustrated in Figure 3(b), the overall performance of the simplified hydraulic model is very reasonable, and the estimate $\hat{p}_c$ is able to follow the general trend of the measured pressure p_c. These results demonstrate that the proposed control-oriented model is, indeed, a good candidate for capturing the fundamental dynamics of the hydraulic part of the BBW actuator.

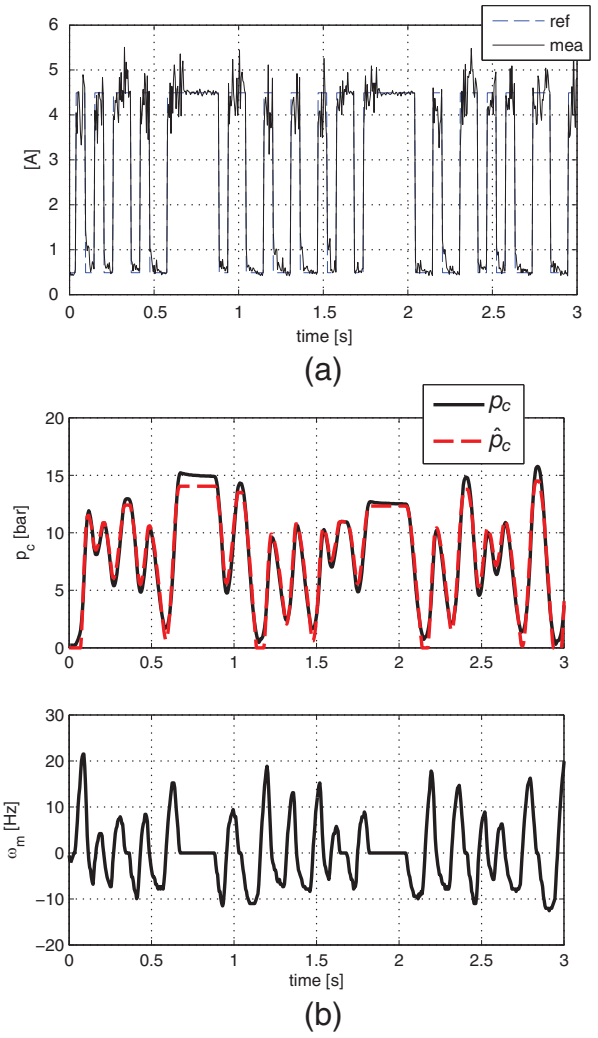

Figure 3. Experimental validation of the hydraulic sub-block of the control-oriented model (note that in this test, ω_m is regarded as the pseudo-input for the hydraulic model, while p_c is the output). (a) Input current and (b) identification test: p_c– measured pressure and $\hat{p}_c$– estimated from the model.

Friction characterization and modelling

After establishing a practical model for the BBW actuator, we will now characterize in more detail the friction disturbance T_f. From a physical point of view, friction is an ubiquitous phenomenon that is present in almost every part of the BBW actuator, being particularly intense in the reduction gear–ball-screw system

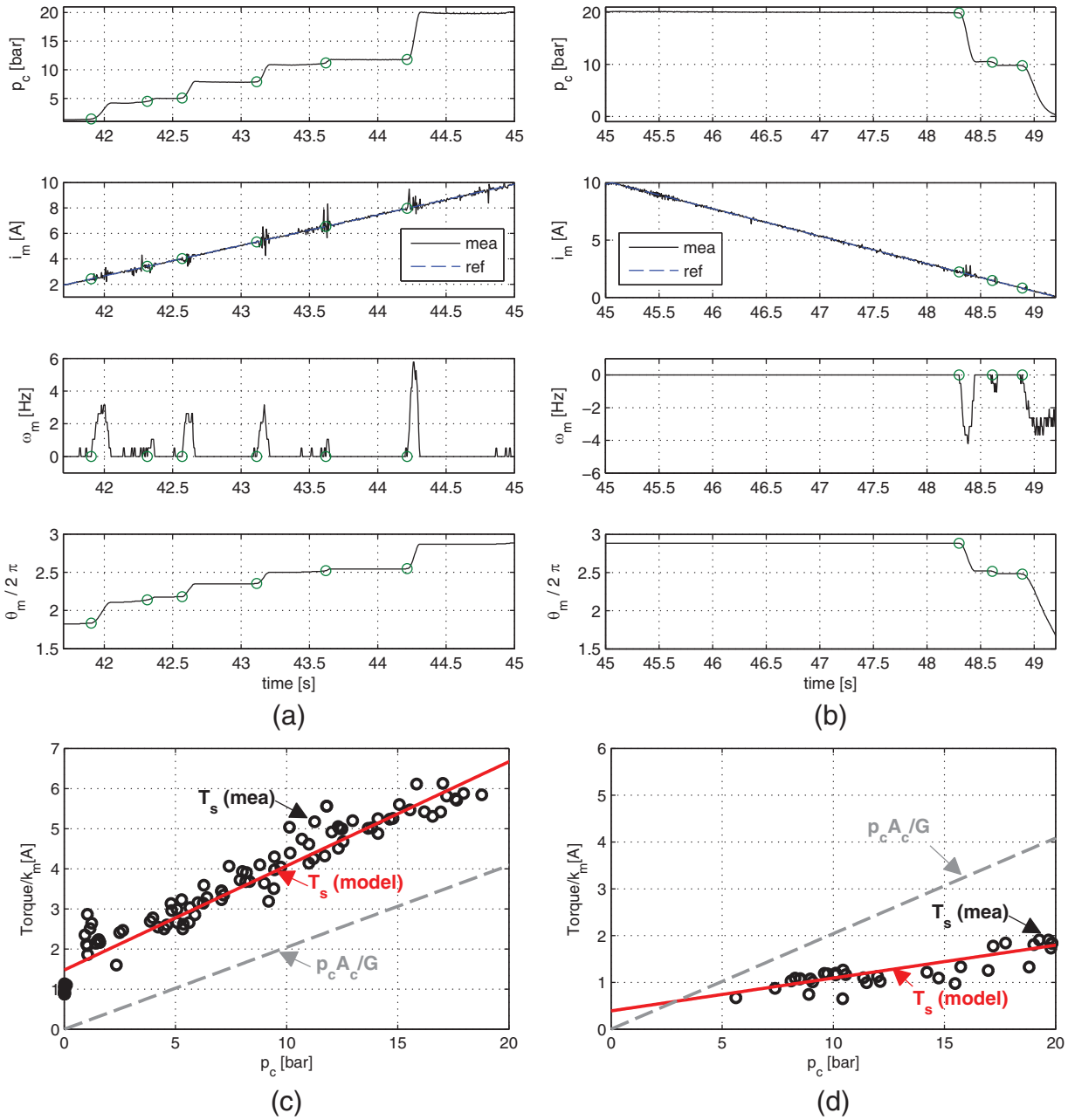

Figure 4. Experimental characterization of the breakaway torque in the BBW actuator.
For convenience, the torque variables are translated to current using the current/torque motor gain k_m and the circles represent the time instances where the breakaway occurs. a), c): characterization of the breakaway torque during positive torque steps ($di_m/dt > 0$). b), d): characterization of the breakaway torque during negative torque steps ($di_m/dt < 0$).

(due to the high reduction ratio) and in the master cylinder (as a result of tight sealing used in the cylinder). In order to gain some insight on how this issue affects our application, a series of open-loop experiences in the BBW actuator were prepared. The idea was to apply a relatively slow ramp (2.4 A/s) to the motor current and observe the response of the system states, such as motor speed and hydraulic pressure. As can be seen in Figure 4(a), the BBW actuator exhibits the typical stick-slip motion, which can be qualitatively described as follows: (1) the increasing motor torque eventually overcomes the static friction load (see the circles in Figure 4(a)) and starts moving the master cylinder's piston (slip phase); (2) by pushing the piston, the pressure in the master cylinder increases, which in turn raises the motor load, and more importantly, the friction levels (as we will see shortly, friction displays a load-dependent behaviour); and (3) this increment in the total load will, at some point, surpass the motor torque, which will decelerate the piston and, ultimately, stop it (stick phase). This stick-slip pattern then repeats periodically throughout the test.

Besides the qualitative analysis of the actuator motion, this open-loop test can also be explored to infer the values of breakaway friction torque, that is, the minimum value that will overcome the static friction. Towards that goal, it is necessary to estimate the friction torque and the time instants where the breakaway happens. The first estimative can be performed with the help of the relation (18a), while the breakaway's time instants are defined as

$$\Omega = \{t | \omega_m(t - i) = 0,\ \omega_m(t + i) > 0,\ \forall i \in (0, \bar{T}]\}$$

where $\bar{T}$ is the length of a time window where the piston motion is evaluated. For illustration purposes, the Ω set is highlighted by circles in Figure 4. Assuming that the motor acceleration ($\dot{\omega}_m$) is relatively low in the domain Ω, thus the term $J_{eq}\dot{\omega}_m$ can be neglected in equation (18a), the breakaway torque T_S can be approximated by

$$T_S(t) \approx k_m i_m(t) - \tfrac{A_c}{G} p_c(t), \quad t \in \Omega \tag{21}$$

Figure 4(c) shows the experimental results obtained with this estimator, plotted against the pressure p_c, during the rising part of the current ramp (i.e. $di_m/dt > 0$). These results suggest that T_S increases with the pressure in the master cylinder p_c. To some extent, this is a reasonable behaviour since the type of actuator under study is expected to display 'load-dependent' friction, as explained in Mare.[32] Furthermore, taking into account the (almost) linear increase in T_s with the p_c, as shown by the experimental data, it is appropriate to consider an affine model for the breakaway torque T_s, which is

$$\hat{T}_S(p_c) = T_{S0} + T_{Sp} p_c \tag{22}$$

where T_{S0}, T_{Sp} are parameters. As shown in Figure 4(c), there is a reasonable agreement between the measurements and this affine model. Another point worth stressing is related to the control effort that the motor needs to develop to overcome the (static) friction. To better explain this point, recall that, in steady-state conditions ($\dot{\omega}_m = 0$), and in light of equation (18a), we will have the following condition

$$k_m i_m = \frac{A_c}{G} p_c + T_f \tag{23}$$

This means that the torque developed by the motor ($k_m i_m$) will be used to generate the braking pressure ($(A_c/G)p_c$) and overcome the friction disturbance T_f. Now, looking again at Figure 4(c), we can observe that the (breakaway) friction disturbance is significantly higher (2–3 times) than the expected load torque associated with the braking pressure. This result clearly emphasizes the dominant role that friction disturbance has in the BBW actuator.

It is also useful to analyse the results of the open-loop test when the motor current is decreasing ($di_m/dt < 0$), as shown in Figure 4(b). The most striking result to emerge from the data is that, for $t \in [45, 48.3]s$, the motor current diminishes from 10 (equivalent to 100% of the nominal torque) to 2 A, but the motor position and the pressure remain unchanged. This loss of control authority can be explained, again, by the strong effect of friction. Interestingly, the breakaway torque for this situation ($\omega_m < 0$) shows much lower friction levels than the situation where the piston is being pushed (see Figure 4(d)), which puts in evidence the large friction asymmetries in the actuator.

Friction map

The analysis carried out thus far has focused on the characterization of the breakaway friction torque. We will now move our attention to the friction study when the actuator is moving, that is, $|\omega_m| > 0$. In this operation mode, the most relevant factors that need to be considered are the well-known Coulomb friction, viscous friction, and Stribeck effects.[17] Classically, these factors can be modelled through a static map, having as main input the speed difference between the contact bodies in the actuator (ω_m). In addition, given the load-dependent friction that affects the actuation, illustrated in Figure 4, it seems appropriate to also conjecture the possibility of having some terms in the friction map that increase linearly with hydraulic pressure p_c. Accordingly, the friction map under consideration for the BBW actuator is given by

$$\begin{aligned} T_f(\omega_m, p_c) = {} & (T_{C0} + T_{Cp} p_c) sgn(\omega_m) + \sigma_2 \omega_m \\ & + \Delta T e^{-\left(\frac{\omega_m}{\omega_s}\right)^2} sgn(\omega_m) \end{aligned} \tag{24}$$

where T_{C0} is the (no-load) Coulomb friction torque, T_{Cp} is the Coulomb friction increase due to pressure in the master cylinder, ΔT is a torque difference between the breakaway and the Coulomb torque, ω_s is the Stribeck speed, and σ_2 is the viscous friction coefficient.

Notice that, in practice, the hydraulic pressure affects not only the Coulomb term but also the viscous and Stribeck terms, that is, the parameters σ_2 and ΔT may change with p_c. However, we verified that the load dependence is more pronounced in the Coulomb term, and to avoid over-complicating the friction model, the load effects in the viscous and Stribeck terms were neglected. Another aspect needing special attention is the friction asymmetries with respect to the direction of movement. To address this issue, the model's parameters in equation (24) must be switched in accordance with the direction of movement, that is

$$\circ = \begin{cases} \circ^+, & \text{if } \omega_m > 0 \\ \circ^-, & \text{otherwise} \end{cases} \tag{25}$$

where '$\circ$' represents one of the parameters $T_{C0}, T_{Cp}, \sigma_2, \Delta T$, and ω_s.

Towards the experimental validation of equation (24), we arranged another series of open-loop experiments with the BBW actuator, which follows a similar

Table 2. Nominal values of the friction model.

Mode	T_{C0} (A)	T_{Cp} (A/bar)	σ_2 (A/rad/s)	ΔT (A)	ω_s (rad/s)
$\omega_m > 0$	1.28	0.23	0.0065	1.12	6.9
$\omega_m < 0$	0.16	0.05	0.0023	0.97	5.6

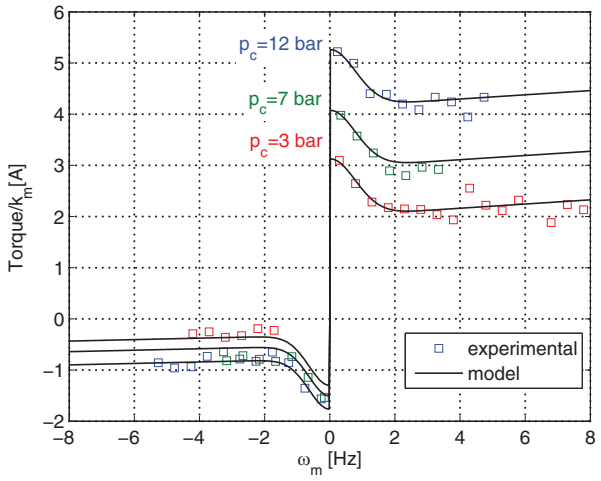

Figure 5. Comparison between the experimental friction map and the model (24).

pattern to those employed in the breakaway test. More specifically, after imposing in the motor current a ramp setpoint (2.4 A/s), the pressure and speed measurements were used to estimate the friction torque through the relation (18a). The experimental results depicted in Figure 5 show two features that were already noticed in the breakaway torque tests, namely, (1) the friction torque increases with the hydraulic pressure p_c and (2) the direction of motion plays a major role in the friction levels (in particular, the friction disturbance is much more severe in the domain $\omega_m > 0$). Moreover, by fitting the experimental data with equation (24), we can also observe a very satisfactory agreement between the measures and the friction model (the parameters of the model, obtained with non-linear fitting techniques, are shown in Table 2).

Remark 1. It is a well-known fact that the friction map (24) will not be able to capture some features of the friction disturbance, such as presliding displacement, frictional lag, or the variable breakaway force.[17] To represent these features, we would need to use a more complicated friction model, such as the LuGre model.[32,33] Nonetheless, our main focus here is to employ practical control-oriented models, which, albeit providing only an approximation of the reality, are easier to treat at the control design stage. As a result, we will assume that the friction can be modelled by a static map and endow the BBW controller with robust mechanisms to cope with modelling errors.

A practical LP for friction compensation

The friction torque model (24), in addition to the non-linearities, also depends on a set of parameters $(T_{C0}, T_{Cp}, \sigma_2, \Delta T, \omega_s)$ that are subject to uncertainty. In order to facilitate the effective handling of this uncertainty by the BBW controller, we will present in this section an LP model, suitable for (model-based) friction compensation with adaptive methods. With this objective in mind, it is worth highlighting the fact that the parameters $(T_{C0}, T_{Cp}, \sigma_2)$ have a linear effect in equation (24), and as a result, they are already in a proper format to be incorporated in the LP. However, the exponential $f_e(\omega_m, \omega_s) = e^{-(\omega_m/\omega_s)^2}$, related to the Stribeck effect, is nonlinear in the parameter ω_s. In order to derive an LP to this term, in the sequel, we will consider that the Stribeck speed is constrained to the domain: $\underline{\omega_s} \leqslant \omega_s \leqslant \overline{\omega_s}$.

Normalization of the Stribeck effect. In general, the Stribeck speed is a parameter that varies from application to application and is subject to a wide range of variation, for example, Armstrong et al.[34] argue that ω_s can vary between 0.00001 and 0.1 m/s (equivalent linear motion). To keep our approach general, it is useful to introduce a normalization factor in the parameter ω_s. With this goal in mind, let us re-parameterize the ω_s range as

$$\omega_s \in [\underline{\alpha}\hat{\omega}_s, \bar{\alpha}\hat{\omega}_s] = [\underline{\omega_s}, \overline{\omega_s}] \tag{26}$$

where $\hat{\omega}_s \in [\underline{\omega_s}, \overline{\omega_s}]$ is the (nominal) estimative for the Stribeck speed and $\underline{\alpha} \in (0, 1], \bar{\alpha} \in (1, \infty)$ are selected in order to keep the original range intact. Introducing this normalization in the exponential term

$$f_{en}(\omega_m, \alpha) = f_e(\omega_m, \alpha\hat{\omega}_s) = e^{-\left(\frac{1}{\alpha}\right)^2\left(\frac{\omega_m}{\hat{\omega}_s}\right)^2} \tag{27}$$

where $\alpha \in [\underline{\alpha}, \bar{\alpha}]$, and defining the additional normalization variables

$$X = \left(\frac{\omega_m}{\hat{\omega}_s}\right)^2, \ \eta = \left(\frac{1}{\alpha}\right)^2 \tag{28}$$

the non-linear Stribeck effect can be represented with the equivalent function

$$f(X, \eta) = e^{-\eta X} \tag{29}$$

where $\eta \in [\underline{\eta}, \bar{\eta}] = \left[1/(\alpha)^2, 1/(\underline{\alpha})^2\right]$ is an unknown parameter, which models the uncertainty in the estimation $\hat{\omega}_s$, and X the normalized input.

Remark 2. Normally, the Stribeck effect is represented by the generic expression $e^{-|\omega_m/\hat{\omega}_s|^{\chi}}$, with typical values of $\chi = 1$ (Tustin model), $\chi = 2$ (Gaussian model), and in general $\chi \in [0.5, 1] \cup \{2\}$.[34,35] In this work, it was assumed that $\chi = 2$, but the described method to derive the optimal LP can easily be adapted to other values of χ, by changing the normalized variables as $X = |\omega_m/\hat{\omega}_s|^{\chi}$, $\eta = 1/\alpha^{\chi}$.

Formulation of the optimal LP problem. To approximate equation (29) with an LP, we will consider functions with the following format

$$f_{LP}(X, \theta, \mathbf{w}) = \underbrace{\begin{bmatrix} h_1(X, \mathbf{w}) & \dots & h_d(X, \mathbf{w}) \end{bmatrix}}_{h^T(X, \mathbf{w})} \theta \tag{30}$$

where $h_i(X, \mathbf{w}), i = 1, \dots, d$ are the basis functions, $\theta \in \mathbb{R}^d$ are the linear parameters, and $\mathbf{w} \in \mathbb{R}^m$ are the weights that characterize the (possible) non-linear basis functions. The selection of these weights will be carried out through the following procedure.

Proposition 1. The weight $\mathbf{w}^*$ that minimizes the fitting error between the LP $f_{LP}(X, \theta, \mathbf{w}^*)$ and $f(X, \eta)$ over the parametric range of interest $(X, \eta) \in [0, \overline{X}] \times [\underline{\eta}, \overline{\eta}]$ is defined as the solution of the following optimization problem

$$\begin{aligned} &\min_{\mathbf{w} \in \mathbb{R}^d} \varepsilon_T(\mathbf{w}) \\ &\text{s.t.} \quad \epsilon_T(\mathbf{w}) = \int_{\underline{\eta}}^{\overline{\eta}} (\epsilon(\eta, \mathbf{w}) d\eta) \\ &\epsilon(\eta, \mathbf{w}) = \int_0^{\overline{X}} \left(f(X, \eta) - \mathbf{h}^T(X, \mathbf{w}) \mathbf{G}^{-1}(\mathbf{w}) \mathbf{c}(\eta, \mathbf{w})\right)^2 dX \\ &[\mathbf{G}(\mathbf{w})]_{ij} = \int_0^{\overline{X}} h_i(X, \mathbf{w}) h_j(X, \mathbf{w}) dX \\ &[\mathbf{c}(\eta, \mathbf{w})]_i = \int_0^{\overline{X}} h_i(X, \mathbf{w}) f(X, \eta) dX, \quad i, j = 1, \dots, d \end{aligned}$$

where $\epsilon_T(\mathbf{w})$ is defined as the total fitting error. The motivation and proof of the previous result were derived in De Castro et al.[36]

Numerical evaluation. In the remainder of this article, we will consider that the nominal/estimated Stribeck speed, $\hat{\omega}_s$, has an uncertainty of $\pm 50\%$, which is equivalent to $\underline{\alpha} = 0.5$, $\bar{\alpha} = 1.5$, and $\underline{\eta} = 0.444$, $\bar{\eta} = 4$. Furthermore, we fixed $\bar{X} = 5$ since this is generally enough to cover the range where the Stribeck effect is pronounced. Due to the exponential nature of the Stribeck curve, the basis functions employed in this work also rely on exponentials

$$\boldsymbol{h}_E(X, \mathbf{w}) = \begin{bmatrix} e^{-w_1 X} & e^{-w_2 X} & \dots & e^{-w_d X} \end{bmatrix}^T \tag{31}$$

Next, the problem described in Proposition 1 was discretized and then tackled with a numerical solver,[37] which enabled us to obtain the optimal weights $\mathbf{w}^*$.

Table 3. Total error ε_T for fitting equation (29) with different LPs.

Basis function	Number of basis (d)		
	1	2	3
Lorentzian[23]	0.2833	–	–
Mixed exponentials[19]	–	0.0224	–
Polynomial[21,22]	–	0.197	0.0256
Exponentials	0.0976	0.0087	0.0004

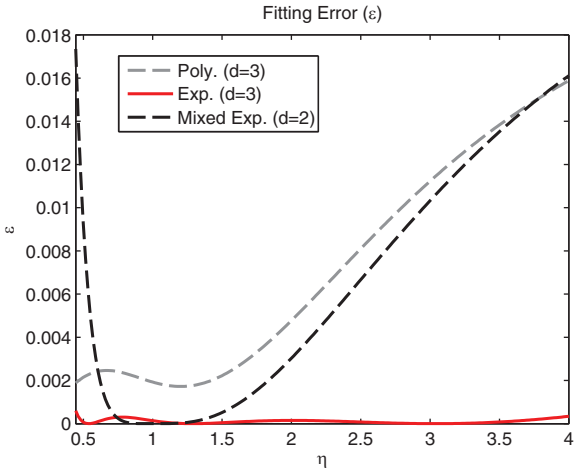

Figure 6. Fitting error $\epsilon(\eta, \mathbf{w}^*)$ evaluated for polynomials, exponentials, and mixed exponentials (see Table 3).

To investigate the performance of the optimal LP, Table 3 represents the total fitting error metric, $\epsilon_T(\mathbf{w})$, evaluated for different types (and number) of basis functions. It is interesting to note that, from the LPs previously proposed in the literature, the mixed exponentials (MEs)[19] provide a respectable fitting result when compared with the Lorentzian function[23] and the polynomial approach.[21,22] Nevertheless, by employing the fixed exponentials ($\boldsymbol{h}_E$), with the optimal selection of weights, a significant improvement is observed: incorporating two fixed exponentials contributes to a reduction of almost 60% in the total fitting error, while three exponential produces an almost negligible error.

To further investigate the performance of these LPs, Figure 6 shows the evolution of the fitting error, $\epsilon(\eta, \mathbf{w}^*)$, for different values of η. An examination of the ME basis functions shows that the fitting error is almost zero when η approaches 1 (i.e. α is near to 1), implying a small error in $\hat{\omega}_s$. These results are in accordance with the theoretical expectations for this approximation: the MEs were derived based on linearization techniques, thus it should present good results when $\hat{\omega}_s$ is close to the nominal point. These good results, however, do not extend to situations when η departs from 1, and the ME ends up introducing significant fitting errors. On the contrary, it can be observed that when fixed exponentials ($d = 3$) are employed, the fitting

error is almost zero everywhere, which highlights the robustness of this LP against uncertainty in η (or in $\hat{\omega}_s$ estimation).

In summary, the optimal LP for approximating the normalized Stribeck effect (29) was found to be exponential based, with $d = 3$

$$\boldsymbol{h}_{E3}(X) = \begin{bmatrix} e^{-0.538X} & e^{-1.289X} & e^{-3.043X} \end{bmatrix}^T \tag{32}$$

This enables us to approximate the original non-linear friction map (24) with the following LP

$$\begin{aligned} T_f(\omega_m, p_c) &= \theta^T \varphi(\omega_m, p_c) sgn(\omega_m) \\ \varphi(\omega_m, p_c) &= \begin{bmatrix} 1 & p_c & |\omega_m| & h_{E3}^T \left(\left(\frac{\omega_m}{\bar{\omega}_s} \right)^2 \right) \end{bmatrix}^T \end{aligned} \tag{33}$$

where $\theta \in \mathbb{R}^n$, $n = 6$, and $\varphi(\omega_m) sgn(\omega_m)$ is the regressor.

Two important factors should be taken into consideration when implementing the above LP. First, the regressor function depends on the discontinuous function $sgn(\omega_m)$, which makes the numerical calculation of this regressor sensitive to measurement errors and may excite high-frequency modes neglected during the modelling phase.[38] To mitigate this issue, the term $sgn(\omega_m)$ will be approximated by a continuous function, based on a logistic sigmoid $c(\omega_m) = -1 + 2/(1 + e^{-k_c \omega_m})$, $k_c > 0$. This allows us to approximate the LP through the following continuous map

$$T_f(\omega_m, p_c) \approx \theta^T \Phi(\omega_m, p_c) \tag{34a}$$

$$\Phi(\omega_m, p_c) = \varphi(\omega_m, p_c) c(\omega_m) \tag{34b}$$

The second factor that deserves special attention is related to the asymmetric levels of friction present in the actuator. These asymmetries make it convenient to switch the parameters of the LP according to the direction of motion, that is

$$\theta = \begin{cases} \theta^+, & \text{if } \omega_m > 0 \\ \theta^-, & \text{otherwise} \end{cases} \tag{35}$$

where θ^+ and θ^- are the friction parameters associated with positive and negative speeds, respectively.

Controller design

In this section, a control strategy for the BBW braking actuator will be developed. The control objective is a tracking one: design a control law for the motor current u such that the hydraulic pressure $x_3 = p_c$ follows, as fast as possible, the reference x_3^*.

This pressure setpoint, normally defined by the driver or by an auxiliary safety system (like the antilock braking system (ABS)), is supposed to have known first ($\dot{x}_3^*$) and second ($\ddot{x}_3^*$) time derivatives. In accordance with the discussion presented in the previous sections, the design of this controller will rely on the reduced model (18) and on the optimal LP (34), that is

$$\dot{x}_2 = \frac{1}{J_{eq}} \left(k_m u - \alpha_3 x_3 - \theta^T \Phi(x_2, x_3) \right) \tag{36a}$$

$$\dot{x}_3 = \frac{\alpha_2}{\alpha_1} x_2 + \delta(t) \tag{36b}$$

$$y = x_3 - x_3^* \tag{36c}$$

where y is the model output and $\alpha_3 = A_c/G$.

Input–output linearization and normal form

To gain additional insight regarding the model (36), it is helpful to determine its relative degree. Recall that, generally, the relative degree of a single-input-single-output system is equal to the number of times the output y needs to be differentiated until the control input u appears, for the first time, in the derivatives of y.[39] By considering the first and second time derivatives of the output

$$\begin{aligned} \dot{y} &= \dot{x}_3 - \dot{x}_3^* = \tfrac{\alpha_2}{\alpha_1} x_2 + \delta(t) - \dot{x}_3^* \\ \ddot{y} &= \underbrace{\frac{\alpha_2}{\alpha_1 J_{eq}}}_{w^{-1}} \left(k_m u - \alpha_3 x_3 - \theta^T \Phi(.) + \underbrace{\frac{\alpha_1 J_{eq}}{\alpha_2} \dot{\delta}(t)}_{\gamma(t)} \right) - \ddot{x}_3^* \\ &= \tfrac{1}{w} \left(k_m u - \alpha_3 x_3 - \theta^T \Phi(x_2, x_3) + \gamma(t) \right) - \ddot{x}_3^* \end{aligned} \tag{37}$$

it can be concluded that the actuator has relative degree 2. Furthermore, according to the input–output (IO) linearization technique, the non-linear terms in the previous relation can be cancelled by selecting the control input as

$$k_m u = \alpha_3 x_3 + \theta^T \Phi(x_2, x_3) - \gamma(t) + w(v + \ddot{x}_3^*) \tag{38}$$

where v is a new control term. Replacing this law in equation (37) produces a second-order linear dynamic, that is, $\ddot{y} = v$, which can straightforwardly be stabilized by a suitable selection of v. Moreover, given that equation (36) has relative degree 2 (equal to the number of states), this control-oriented model does not have zero dynamics. This result is also evident from the normal form associated with the reduced model (36)

$$\begin{aligned} \dot{e}_1 &= e_2 \\ \dot{e}_2 &= \tfrac{1}{w} \left(k_m u - \alpha_3 x_3 - \theta^T \Phi(x_2, x_3) + \gamma(t) - w \ddot{x}_3^* \right) \end{aligned} \tag{39}$$

where $e_1 = y = x_3 - x_3^*$ and $e_2 = \dot{y}$.

Adaptive-robust controller

The control law (38), although effective in handling the model non-linearities, is dependent on the exact knowledge of the friction parameters (θ) and it needs the value of the function $\gamma(t)$. In practice, both θ and $\gamma(t)$ may change throughout the actuator's operation conditions (e.g. with temperature, mechanical wear) and are also subject to uncertainty. To cope with these uncertainties, the ideal controller will be modified in two directions. First, adaptive mechanisms will be included in the controller to deal with the parametric uncertainty in θ, and second, $\gamma(t)$ will be treated as a disturbance that the controller should robustly attenuate.

Taking into account the normal form (39), the design of this adaptive-robust controller can be simplified by using a 'sliding-like' variable s

$$s = e_2 + L_1 e_1 \tag{40}$$

where L_1 is a positive constant. It is easy to see that if s is maintained at zero, then the pressure error will decrease to zero with a first-order dynamic, that is, $e_1 = -L_1 e_1$. Consequently, the controller design can be based on the s variable, which is a common practice in servo control applications.[18,26,38] For control design purposes, it is also convenient to determine the sliding variable dynamics

$$\dot{s} = \frac{1}{w}\left(k_m u - \alpha_3 x_3 - \theta^T \Phi(x_2, x_3) + \gamma(t) - w(\ddot{x}_3^* - L_1 e_2)\right) \tag{41}$$

In order to stabilize this s dynamic, we propose the following control law

$$\begin{aligned} k_m u = {} & \alpha_3 x_3 + \hat{\theta}^T \Phi(x_2, x_3) + \hat{w}(\ddot{x}_3^* - Le_2) \\ & - \rho \tanh\left(\frac{s}{\varepsilon}\right) - L_2 s \end{aligned} \tag{42}$$

where L_2 is a positive tuning constant, and $\hat{\theta}$ and $\hat{w}$ are estimates of θ and w, which will be defined by an adaptive mechanism (to be introduced shortly). From an engineering standpoint, the structure of the proposed controller can be explained as follows. The first two terms attempt to cancel the load torque resulting from the friction and the generation of the hydraulic braking pressure. The third term appears due to tracking formulation of the problem and the sliding variable definition. The fourth term employs a continuous sliding mode action to attenuate the effect of the disturbance $\gamma(t)$, where $\varepsilon > 0$ is the width of the boundary layer. Finally, the last term is incorporated to improve the transient response.

At this stage, it is worth pointing out that, besides the friction parameters $\hat{\theta}$, the proposed controller will also perform an online adaptation of the w parameter. From a practical perspective, this adaptation is also relevant because w constitutes another source of parametric uncertainty (e.g. w depends on the pad's stiffness k_p, which, as already discussed, varies in time). With regard to the other two parameters in the control law (k_m, α_3), we treat them as known constants. In our view, this approach is justified by the fact that both variables are known with a reasonable accuracy, for example, $\alpha_3 = A_c/G$ depends only on the geometric properties of the actuator, whereas the current/torque gain k_m is generally a well-known quantity.

Stability and adaptive laws

As commonly done in the construction of robust controllers, we will work under the premise that the disturbance $\gamma(t)$ and the parameters θ and w are upper bounded

$$|\gamma(t)| = \left|\frac{\alpha_1 J_{eq}}{\alpha_2}\dot{\delta}(t)\right| \leqslant \frac{\alpha_1 J_{eq}}{\alpha_2}\bar{\delta}_1 \leqslant \rho \tag{43}$$

$$0 < w \leqslant M_w,\ \|\theta\| \leqslant M_\theta \tag{44}$$

where ρ, M_w, and M_θ are constants. To investigate the stability of the proposed adaptive-robust controller, as well as to find the adaptive laws for the parameters' estimates $\hat{\theta}$ and $\hat{w}$, consider the following candidate Lyapunov function

$$V(s, \tilde{\theta}, \tilde{w}) = \frac{w}{2}s^2 + \frac{1}{2}\tilde{\theta}^T \Gamma_\theta^{-1}\tilde{\theta} + \frac{1}{2\Gamma_w}\tilde{w}^2 \tag{45}$$

where $\tilde{\theta} = \hat{\theta} - \theta$ and $\tilde{w} = \hat{w} - w$ represent the parametric estimation errors, and Γ_θ and Γ_w are positive-definite gains. Calculating the time derivative of V, it can be shown that

$$\begin{aligned} \dot{V} = {} & -L_2 s^2 + \tilde{\theta}^T\left[\Phi(x_2, x_3)s + \Gamma_\theta^{-1}\dot{\tilde{\theta}}\right] \\ & + \tilde{w}\left[(\ddot{x}_3^* - Le_2) + \Gamma_w^{-1}\dot{\tilde{w}}\right] + s\left[\gamma(t) - \rho\tanh\left(\frac{s}{\varepsilon}\right)\right] \end{aligned} \tag{46}$$

The adaptation law adopted in this work is based on the switching-σ method[40]

$$\begin{aligned} \dot{\hat{\theta}} = {} & -\Gamma_\theta\left(\Phi(x_2, x_3)s + \sigma_\theta(\hat{\theta})\hat{\theta}\right), \\ \sigma_\theta = {} & \begin{cases} 0, & \text{if } \|\hat{\theta}\| \leqslant M_\theta \\ \sigma_0, & \text{otherwise} \end{cases} \\ \dot{\hat{w}} = {} & -\Gamma_w\left(s(\ddot{x}_3^* - Le_2) + \sigma_w(\hat{w})\hat{w}\right), \\ \sigma_w = {} & \begin{cases} 0, & \text{if } |\hat{w}| \leqslant M_w \\ \sigma_0, & \text{otherwise} \end{cases} \end{aligned} \tag{47}$$

where $\sigma_0 > 0$ is a tuning parameter. The idea behind the switching terms is to introduce leakage in the integration process of the adaptation law, whenever excessive estimates are present. This leakage ends up attenuating the parameter-drift issues, which is one of the main concerns in this approach. Replacing equation (47) in $\dot{V}$ and by noticing that $|s\gamma(t)| \leqslant \rho|s|$, one has

$$\dot{V} \leqslant -L_2 s^2 - \sigma_\theta(.)\tilde{\theta}^T\hat{\theta} - \sigma_w(.)\tilde{w}\hat{w} + \rho\left(|s| - \tanh\left(\tfrac{s}{\varepsilon}\right)s\right)$$

Now, consider the following auxiliary results

$$\begin{aligned} \text{(a)}\quad -\sigma_\theta(.)\tilde{\theta}^T\hat{\theta} \leqslant {} & -\sigma_0\tilde{\theta}\hat{\theta} + 2\sigma_0 M_\theta^2 \leqslant -\frac{\sigma_0}{2}\|\tilde{\theta}\|^2 \\ & + \frac{\sigma_0}{2}\|\theta\|^2 + 2\sigma_0 M_\theta^2 \end{aligned} \tag{48}$$

$$\begin{aligned} \text{(b)}\quad -\sigma_w(.)\tilde{w}\hat{w} \leqslant {} & -\sigma_0\tilde{w}\hat{w} + 2\sigma_0 M_w^2 \leqslant -\frac{\sigma_0}{2}\tilde{w}^2 \\ & + \frac{\sigma_0}{2}w^2 + 2\sigma_0 M_w^2 \end{aligned} \tag{49}$$

$$\text{(c)}\quad 0 \leqslant |s| - s\tanh\left(\frac{s}{\varepsilon}\right) \leqslant 0.2785\varepsilon = \tilde{k}\varepsilon \tag{50}$$

The first inequality of equations (48) and (49) is a well-known result for the switching-σ method (Ioannou and Sun,[40] p.561), whereas the second inequality

follows from the completion of squares; inequalities (50) are demonstrated in Farrell and Polycarpou[41] (Lemma A.5.1). Using these three auxiliary results, $\dot{V}$ can be further bounded by

$$\dot{V} \leqslant -L_2 s^2 - \frac{\sigma_0}{2}\left\|\tilde{\theta}\right\|^2 - \frac{\sigma_0}{2}\tilde{w}^2 + \underbrace{\frac{5\sigma_0}{2}\left(M_w^2 + M_\theta^2\right) + \rho\tilde{k}\varepsilon}_{\lambda_2}$$

where $\tilde{k} \geqslant 0.2785$. Selecting $\lambda_1 = \min\left(2L_2/w, \sigma_0/\lambda_{min}(\Gamma_\theta^{-1}), \sigma_0\Gamma_w\right)$, where $\lambda_{min}(\Gamma_\theta^{-1})$ is the smallest eigenvalue of Γ_θ^{-1}, we finally get

$$\dot{V} \leqslant -\lambda_1 V + \lambda_2 \tag{51}$$

This inequality paves the way for the main result of this section.

Proposition 2. Consider the system (41) controlled by equations (42) and (47). The following holds.

1. The signals s, $\hat{\theta}$, and $\hat{w}$ are bounded; in particular

$$|s(t)| \leqslant \sqrt{\frac{2}{w}\max\left(V(0), \frac{\lambda_2}{\lambda_1}\right)} \tag{52}$$

2. The signal s is ultimately bounded by

$$\lim_{t\to\infty}|s(t)| \leqslant \sqrt{\frac{5\sigma_0(M_w^2 + 2M_\theta^2) + 2\rho\tilde{k}\varepsilon}{w \times \min\left(\frac{2L_2}{w}, \frac{\sigma_0}{\lambda_{min}(\Gamma_\theta^{-1})}, \sigma_0\Gamma_w\right)}} \tag{53}$$

Proof. By the comparison Lemma,[39] the differential inequality (51) implies that $V(t)$ is upper bounded by

$$V(t) \leqslant \frac{\lambda_2}{\lambda_1} + e^{-\lambda_1 t}\left(V(0) - \frac{\lambda_2}{\lambda_1}\right) \leqslant \max\left(V(0), \frac{\lambda_2}{\lambda_1}\right) \tag{54}$$

Since $V(t)$ is also lower bounded

$$\frac{w}{2}s^2 + \frac{\lambda_{min}(\Gamma_\theta^{-1})}{2}\left\|\tilde{\theta}\right\|^2 + \frac{1}{2\Gamma_w}\tilde{w}^2 \leqslant V(t) \tag{55}$$

we can conclude that $|s(t)| \leqslant \sqrt{(2/w)V(t)}$, yielding equation (47). The boundedness of the estimates $\hat{\theta}$ and $\hat{w}$ is evident from the 'leaky' integrator adopted in the adaptation law (47). As for the ultimate boundedness of s, it follows from the fact that $\lim_{t\to\infty}|s(t)| \leqslant \lim_{t\to\infty}\sqrt{(2/w)V(t)} \leqslant \sqrt{(2/w)(\lambda_2/\lambda_1)}$.

Experimental validation

The adaptive-robust controller was validated through a series of experimental tests carried out in a test bench. The results are presented and discussed in this section. Throughout these tests, the BBW actuator, already introduced in section 'Actuator model', was controlled through a low-cost digital signal processor (DSP), Freescale MC9S12XE. This controller samples the measurements from the master cylinder's pressure and motor position (through an encoder with 100 pulses per revolution) at a rate of 200 Hz, which is also the execution rate of the pressure controller. The DSP also contains a fast current loop, based on a proportional + integral (PI) control law running at 1000 Hz, which is responsible for regulating the motor current.[12,28] Given that the BBW actuator is a safety critical system, additional measures were considered to detect faults. Accordingly, the DSP unit implements several checks and redundancies: two pressure sensors are available as well as hardware checks on the supply voltage and protection against over-current and short circuit. These solutions, together with a current-loop and pressure-loop observers, are capable of detecting faults in the actuator and to avoid unwanted application of pressure.

In what follows, the presentation and discussion of the experimental tests are divided into four parts. In the first two, we investigate how the proposed adaptive-robust controller performs in comparison with other friction-compensation techniques, namely, (1) proportional + derivative (PD) control law + nominal friction and (2) dither-based friction compensation. The final two experimental tests will show the response of the proposed controller to general setpoints (steps and ramps), as well as real-life braking setpoints.

Nominal versus adaptive friction compensation

As an initial attempt to comply with the control specifications, we start by implementing a simple PD control, with nominal friction compensation. This is a reasonable approach to start with because, in practice, some preliminary experiments can be performed to construct an estimative for the steady-state friction map (as discussed in section 'Friction map'). The PD control law was built from equation (42), with the adaptive mechanism disabled, that is, $\Gamma_\theta = \mathbf{0}$, $\Gamma_w = 0$, gains $L_1 = L_2 = 38$ and fixed estimates $\hat{w} = w$, $\rho = 0$. The (fixed) estimative of the friction parameters $\hat{\theta}$ was obtained by fitting the nominal friction map as shown in Figure 5 with the LP (34). From the sinusoidal tracking results presented in Figure 7(a), one can observe that as long as the friction levels are close to the nominal ones ($t \in [0, 1.5]s$), this control law ensures a satisfactory tracking performance, with pressure error inferior to 1 bar. At $t \geqslant 1.5\,s$, however, the operation window to which the nominal friction model is valid changes (the sine amplitude of the pressure setpoint increases). This introduces a parametric disturbance that the PD controller is unable to handle, generating significant errors in the pressure control (see the time period $t \geqslant 1.5\,s$).

Next, the adaptive-robust controller was evaluated using the parameter configuration specified in Table 4. Just like the PD control, the adaptive law offers good tracking capabilities for the nominal friction situation (see Figure 7(b) for $t \in [0, 1.5]s$). This time, however,

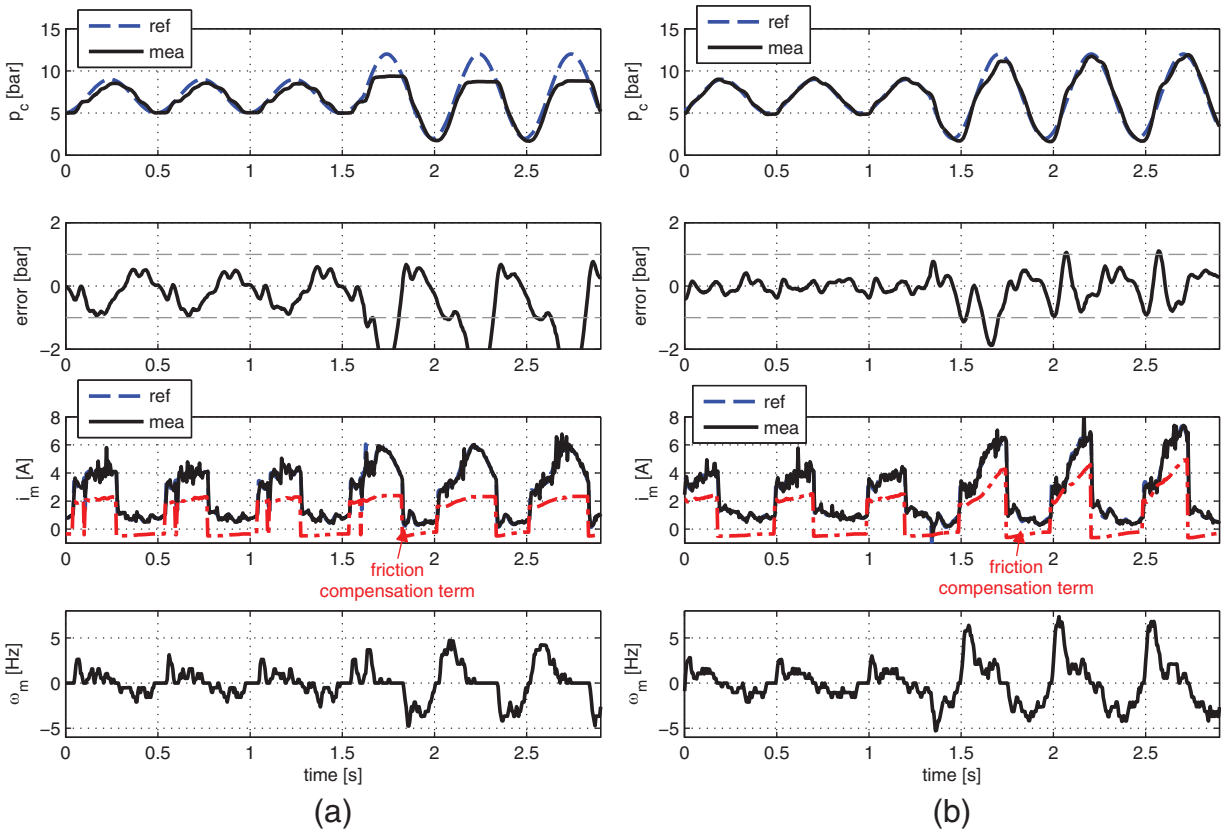

Figure 7. Experimental comparison between two control strategies for tracking the braking pressure: (a) PD with nominal friction compensation and (b) adaptive-robust controller.

Table 4. Controller's parameters.

Variable	Symbol	Value
Controller gain	L_1	38
Controller gain	L_2	38
Upper bound for $\|\gamma(t)\|$	ρ	0.014
Width of boundary layer	ε	150
Leakage factor	σ_0	0.1
Adaptive gains		
$\Gamma_\theta^+ = diag([220.11.41.41.4])\times 10^{-3}$		
$\Gamma_\theta^- = diag([220.11.41.41.4])\times 10^{-4}$		
$\Gamma_w = 10^{-9}$		

Γ_θ^+ represents the adaptation gains employed during positive velocity range and Γ_θ^- contains the gains for the negative velocities.

the proposed controller is able to successfully cope with the parametric disturbance ($t \geqslant 1.5\,s$), showing a quick transient response and low tracking error in steady state. The evolution of the parameter estimation during this test is also represented in Figure 8. For the sake of brevity, we only show the parameter adaptation of the friction parameter $\hat{\theta}^+$ (positive speeds), as these are the ones that have higher uncertainty. Interestingly, these data reveal that, after introducing the setpoint disturbance at $t = 1.5\,s$, there is a significant change in the parameter estimation, particularly in θ_2^+, in an effort to track the new friction conditions. Notice that the main objective of the controller is just the pressure tracking, not parametric estimation (which will only be met if the reference signal has the persistence of excitation property).[18]

Dither versus adaptive friction compensation

Dither is another common approach to mitigate friction disturbances[17] and was used in previous research on the development of BBW control systems.[12,13] The idea behind this technique is to inject in the motor torque a high-frequency auxiliary signal, for example, sinusoidal, such that the actuator is always on the move (or on the verge of movement), in an effort to attenuate the effects of the static friction phenomenon, which is one of the most difficult disturbances with which the controller has to cope. In the scope of the BBW controller development, it is useful to investigate how the model-based friction compensation, employed in our controller, performs in comparison with the dither friction compensation used in previous research. Accordingly, in this section, we compare the performance of the adaptive-robust controller against a PD controller endowed with dither friction compensation. The latter controller is constructed by disabling the friction parameters ($\hat{\theta} = 0$, $\Gamma_\theta = \mathbf{0}$, $\Gamma_w = 0$) and adding a sinusoidal dither term $i_d \sin(\omega t)$ to the control law (42). The parameters of the dither signal, $\omega = 2\pi 71.5\,\mathrm{rad/s}$ and $i_d = \min(7, 4 + p_c)$, were selected based on the previous studies.[12,28]

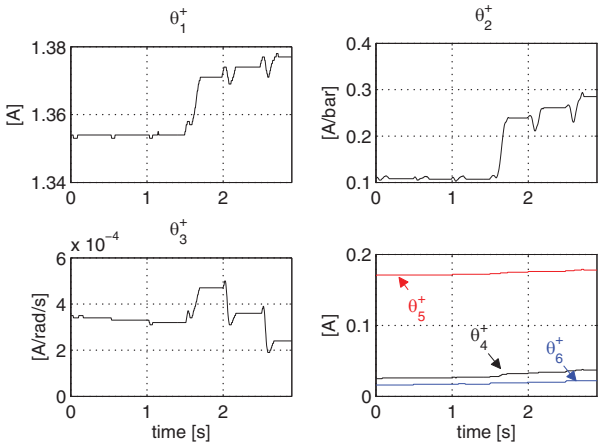

Figure 8. Parameter adaptation of the friction parameters during the experimental test as shown in Figure 7.

From the experimental results shown in Figure 9(a), it can be verified that the pressure responses of the controllers under consideration are very similar. In both cases, the tracking error reaches the ± 1 bar range in approximately 50 ms and the steady state is close to zero. The major differences lie in the control action, that is, the motor current. To keep the motor always on the move, the high-frequency signal injected by the dither generates chattering in the current, which then causes vibrations, audible noise, and, given that the actuator is always moving, that is, $\omega_m \neq 0$, an increase in mechanical wear of the system. On the contrary, the model-based friction compensation does not suffer from such hurdles and produces a much smoother control action. These differences in control action also have an important consequence for the energy consumption in the actuator. As shown in Figure 9(b), the dither controller consumes 13 Ws of electrical energy during the test, whereas the model-based friction compensation (incorporated in the adaptive-robust controller) uses only 7.5 Ws. Hence, these results demonstrate that the model-based friction compensation can reduce the energy consumption of the BBW actuator up to 42.3%. Although energy consumption is not the main priority in the BBW system, the higher energy efficiency offered by the model-based friction compensation is an attractive feature for energy-sensitive applications, as is the case of the automotive field in which the actuator will be employed.

Transient response

After demonstrating the energy and performance advantages of the adaptive-robust pressure controller against other strategies, we investigated more closely the transient response of this controller. Towards that goal, additional experiments with square and triangular waveform setpoints were carried out. It can be seen from the results shown in Figure 10(a) that the transient response to the positive ($2 \rightarrow 10$ *bar*) and negative

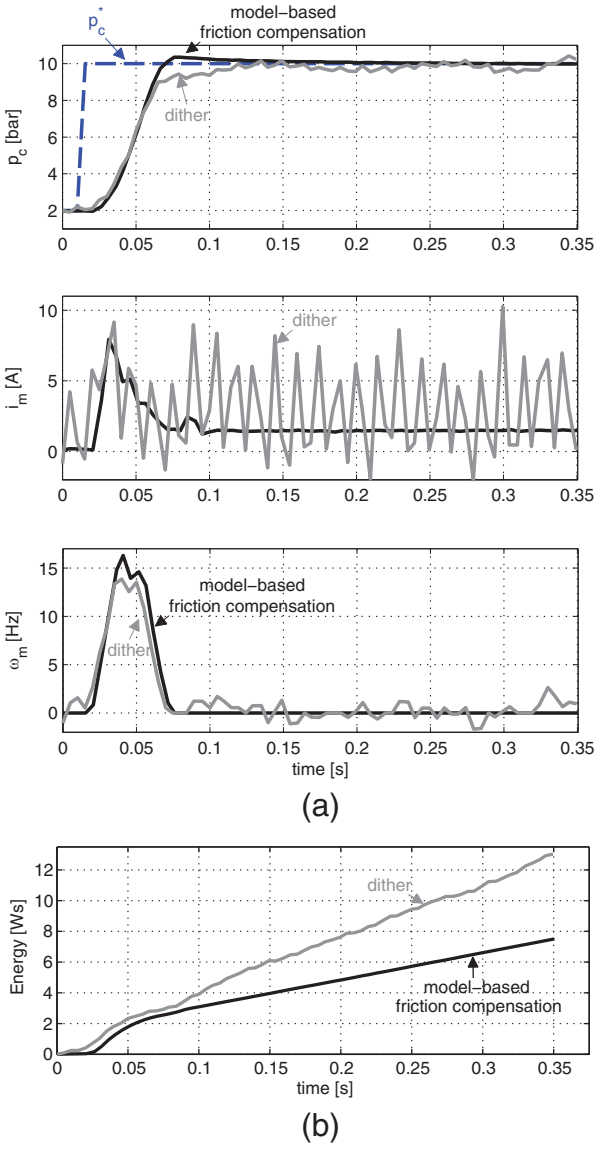

Figure 9. Experimental comparison between the dither technique and the model-based friction compensation (employed in the adaptive-robust controller): (a) transient response and (b) energy consumption of the actuator.

($10 \rightarrow 2$ *bar*) steps is very good. The time to reach the setpoint is less than 50 ms, and the steady-state pressure error is close to zero. There is also a small overshoot during the positive step (0.5 bar), but it still lies within reasonable range.

The response of the controller to ramp setpoints, illustrated in Figure 10(b), also displays a satisfactory performance, with tracking errors below 0.6 bar. From these results, we also can observe that the peak tracking error occurs when the ramp switches from decrease to increase mode (see, for example, $t = 0.26$ s or $t = 1.02$ s). During these time instants, it becomes necessary to reverse the direction of the motor speed ω_m, which is one of the most challenging operation points for the controller, as it will have to cope with the static/breakaway force disturbances.

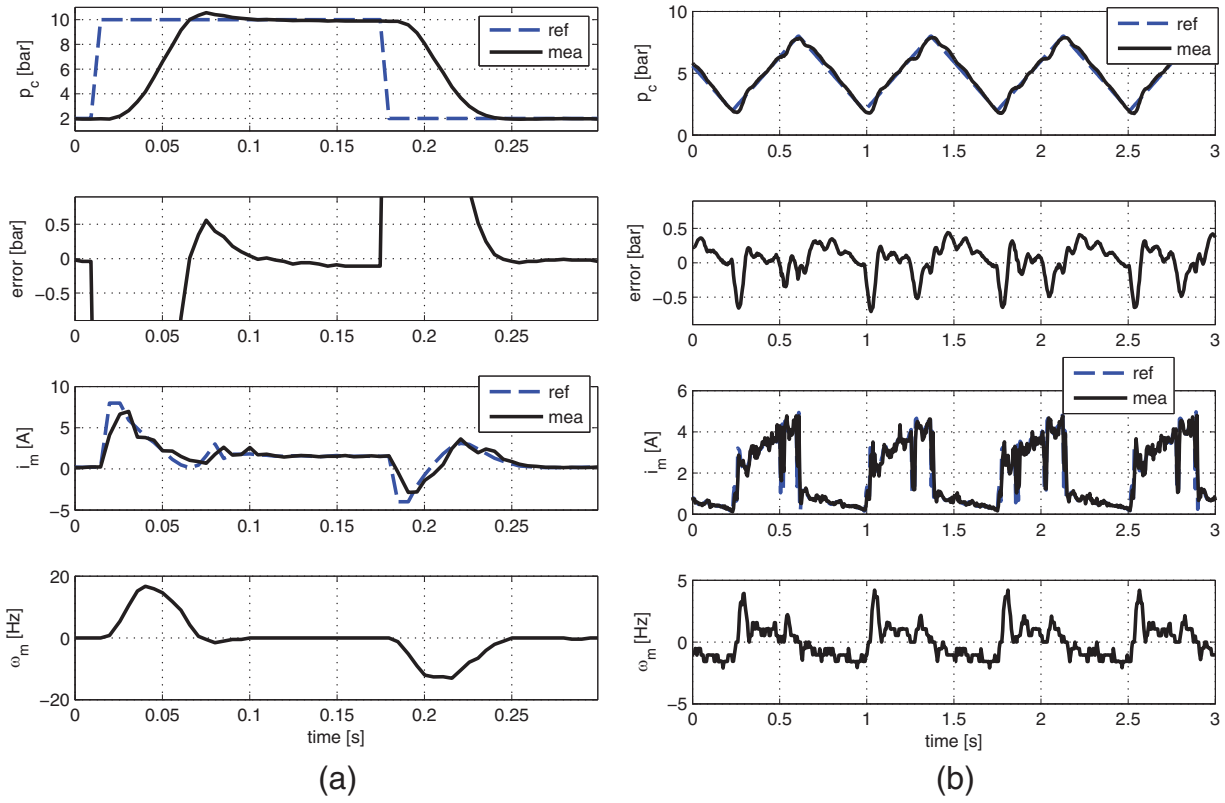

Figure 10. Experimental response of the adaptive-robust controller for step and ramp pressure setpoints: (a) response to steps in the pressure setpoint and (b) response to triangular setpoints.

Validation with realistic setpoints

For the final evaluation of the BBW controller, we employed a pressure setpoint generated by a professional racing pilot, which was acquired during an experimental test session carried out on an instrumented motorbike. Figure 11 shows a typical example of a pressure braking setpoint produced by the racing pilot. This signal can be decomposed into three phases: (1) from $t \in [0, 0.35]$s, we have a strong, and fast, brake increase in the pressure setpoint (35 bar/s); (2) during the modulation phase, $t \in [0.35, 4]$s, the average pressure is kept approximately constant (8 bar in this example), and the driver introduces small oscillations in the braking pressure setpoint in order to seek the maximization of the tyre–road friction force; and (3) finally, for $t \geqslant 4$ s, the driver starts releasing the brakes to allow the vehicle to negotiate the corner.

From an examination of the results presented in Figure 11, it can be concluded that the proposed BBW presents a good tracking performance, with the pressure setpoint being imposed with an accuracy of ± 0.5 bar. As for the control action generated by the controller, one can observe the existence of some current spikes, with amplitude varying between 4 and 6 A. These spikes are a consequence of the high-level (and asymmetric) friction present in the BBW system. For

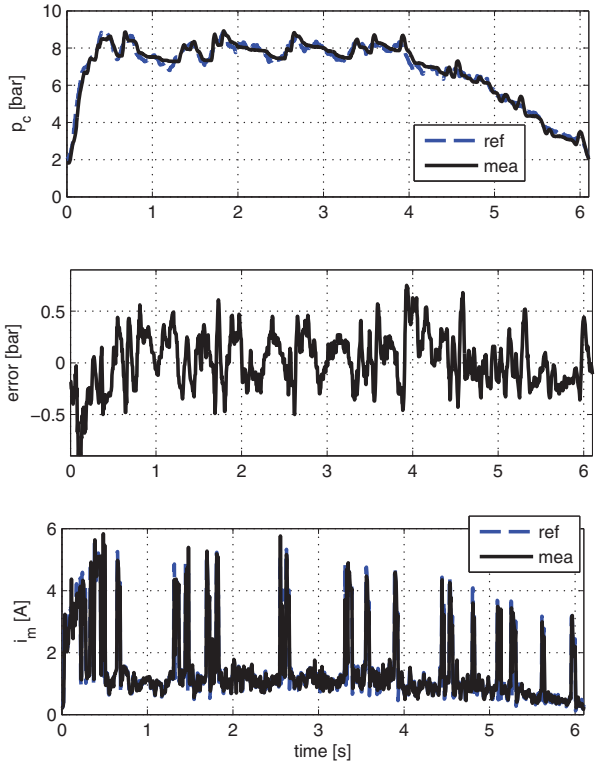

Figure 11. Experimental test of the adaptive-robust controller with a realistic pressure setpoint.

example, given that the friction disturbance is smaller for negative speeds (see the discussion in section 'Friction characterization and modelling'), it is no surprise that during the periods where the pressure setpoint decreases slowly, for example, $t \in [0.72, 1.25] \cup [1.8, 2.5]$s, thus with negative speeds, the motor current is low and relatively smooth (notice that, this behaviour is also present in the tracking of the ramp setpoints, illustrated in Figure 10(b)). However, for the periods of time when the pressure setpoint increases (e.g. $t \in [1.62, 1.82] \cup [2.54, 2.68]$s), and since the friction disturbance for positive speeds is very significant, the controller needs to apply a large control effort, making unavoidable the presence of the current spikes shown in the bottom plot of Figure 11. Despite these difficulties, the experimental tests shown in this section demonstrate that the proposed controller can cope well with the friction disturbances.

Concluding remarks and outlook

In this work, an adaptive-robust controller for tracking the braking pressure of a BBW actuator was proposed. To facilitate the design of this controller, we started by deriving a practical model for the actuator, putting particular focus on the simplification of the hydraulic dynamics. By exploring pragmatic assumptions, we were able to reduce the original actuator model, based on a seven-state representation, to a (uncertain) second-order system. Experimental tests provided strong evidence that this reduced model is able to capture the fundamental dynamics of the actuator, making it very attractive for control purposes. In order to cope with friction disturbance, results from the theory of optimal approximation of functions were used to approximate the non-linear friction map with a simpler and more practical LP. It was shown that compared with the parameterizations previously proposed in the literature, the optimal LP reduces the total fitting error and tolerates a significant uncertainty in all friction parameters, most notably the Stribeck speed. Furthermore, given that the friction (and the LP) is subject to parametric uncertainty, adaptive mechanisms based on switching-σ were incorporated in the BBW controller, while robustness to non-parametric disturbances, arising from modelling simplifications, was handled by a continuous sliding mode action. The stability and ultimate boundedness of the proposed adaptive-robust controller were demonstrated with the help of the Lyapunov method.

The experimental results show that in comparison with the nominal friction-compensation technique, the proposed BBW controller can offer superior robustness to parametric variations. It was also shown that compared with the classical dither-based friction compensation, the proposed controller enables a reduction in the energy consumption of the actuator by more than 40%. Finally, the effectiveness and performance of the adaptive-robust controller were confirmed using realistic pressure setpoints.

It is our intention in future work to address the always important fail-safe operation of the BBW actuator. Towards that goal, we are considering motorcycles' architectures having brake assemblies with two discs/calipers. Our idea is to connect the BBW actuator to one caliper, while the second caliper is manually operated by the rider. In case of a fault, the BBW actuator is shut down and the rider will be still able to operate the brake with one caliper (although with a loss of performance). We also plan to experimentally validate the BBW actuator, and the proposed controller, in a drive-by-wire vehicle.

Acknowledgement

The authors are grateful to Brembo for providing the BBW actuator employed in the experimental tests.

Declaration of conflicting interests

The authors declare that there is no conflict of interest.

Funding

This work was partially funded by the FCT (Science and Technology Foundation), through the scholarship number SFRH/BD/47882/2008.

References

1. Savaresi SM and Tanelli M. *Active braking control systems design for vehicles*. London: Springer-Verlag, 2010.
2. Johansen TA, Petersen I, Kalkkuhl J, et al. Gain-scheduled wheel slip control in automotive brake systems. *IEEE T Contr Syst T* 2003; 11(6): 799–811.
3. Yamakado M, Takahashi J, Saito S, et al. Improvement in vehicle agility and stability by G-Vectoring control. *Vehicle Syst Dyn* 2010; 48(Suppl. 1): 231–254.
4. De Castro R, Araújo RE, Tanelli M, et al. Torque blending and wheel slip control in EVs with in-wheel motors. *Vehicle Syst Dyn* 2012; 50(Suppl. 1): 71–94.
5. Isermann R, Schwarz R and Stolzl S. Fault-tolerant drive-by-wire systems. *IEEE Contr Syst Mag* 2002; 22(5): 64–81.
6. Reuter DF, Lloyd EW, Elliott JA, et al. Hydraulic design considerations for EHB systems. In: *SAE world congress*, Detroit, Michigan, 3–6 March 2003 PA, USA: SAE International.
7. D'alfio N, Morgando A and Sorniotti A. Electro-hydraulic brake systems: design and test through hardware-in-the-loop simulation. *Vehicle Syst Dyn: Int J Vehicle Mech Mobil* 2006; 44(Suppl. 1): 378–392.
8. Kwak J, Yao B and Bajaj A. Analytical model development and model reduction for electromechanical brake system. In: *ASME international mechanical engineering congress and exposition*, Anaheim, CA, 13–20 November 2004. New York: ASME.
9. Line C. *Modelling and control of an automotive electromechanical brake*. PhD Thesis, University of Melbourne, Parkville, VIC, Australia, 2007.

10. Sorniotti A and Repici GM. Hardware in the loop with electro-hydraulic brake systems. In: *Proceedings of the 9th WSEAS international conference on systems*, Athens, Greece, 11–16 July 2005. Stevens Point, WI: WSEAS.
11. Petersen I. *Wheel slip control in ABS brakes using gain scheduled optimal control with constraints*. PhD Thesis, Norwegian University of Science and Technology, Trondheim, 2003.
12. Dardanelli A, Alli G and Savaresi S. Modeling and control of an electro-mechanical brake-by-wire actuator for a sport motorbike. In: *5th IFAC symposium on mechatronic systems*, Marriott Boston Cambridge, USA, 13–15 September 2010. International Federation of Automatic Control (IFAC).
13. Panzani G, Corno M, Todeschini F, et al. Analysis and control of a brake by wire actuator for sport motorcycles. In: *The 13th mechatronics forum international conference*, Linz, Austria, 17–19 September 2012. Austria: Trauner Verlag.
14. Chihoon J, Sungho H and Hyunsoo K. Clamping-force control for electromechanical brake. *IEEE T Veh Technol* 2010; 59(7): 3205–3212.
15. Line C, Manzie C and Good MC. Electromechanical brake modeling and control: from PI to MPC. *IEEE T Contr Syst T* 2008; 16(3): 446–457.
16. Lee CF and Manzie C. Near-time-optimal tracking controller design for an automotive electromechanical brake. *Proc IMechE, Part I: J Systems and Control Engineering* 2012; 226(4): 537–549.
17. Armstrong B and Canudas de Wit C. *Friction modeling and compensation* (ed. WS Levine). Boca Raton, Florida: CRC Press, 1996.
18. Slotine JJE and Li W. *Applied nonlinear control*. Upper Saddle River, NJ: Prentice Hall, 1991.
19. Liu G. Decomposition-based friction compensation of mechanical systems. *Mechatronics* 2002; 12(5): 755–769.
20. Bigras P. Reduced nonlinear observer for bounded estimation of the static friction model with the Stribeck effect. *Syst Control Lett* 2009; 58(2): 119–123.
21. Jatta F, Legnani G and Visioli A. Friction compensation in hybrid force/velocity control of industrial manipulators. *IEEE T Ind Electron* 2006; 53(2): 604–613.
22. Bona B, Indri M and Smaldone N. Rapid prototyping of a model-based control with friction compensation for a direct-drive robot. *IEEE: ASME T Mech* 2006; 11(5): 576–584.
23. Hess DP and Soom A. Friction at a lubricated line contact operating at oscillating sliding velocities. *J Tribol* 1990; 112(1): 147–152.
24. Marton L and Lantos B. Control of robotic systems with unknown friction and payload. *IEEE T Contr Syst T* 2011; 19(6): 1534–1539.
25. Marton L, Fodor S and Sepehri N. A practical method for friction identification in hydraulic actuators. *Mechatronics* 2011; 21(1): 350–356.
26. Marton L and Lantos B. Modeling, identification, and compensation of stick-slip friction. *IEEE T Ind Electron* 2007; 54(1): 511–521.
27. De Castro R, Araújo RE and Freitas D. Adaptive compensation of the Stribeck friction in brake-by-wire actuators. In: *The 13th mechatronics forum international conference*, Linz, Austria, 17–19 September 2012. Trauner Verlag.
28. Acquistapace A and Mazzoleni S. *Modellistica e controllo di un impianto frenante brake-by-wire per motocicli ad alte prestazioni*. Master Thesis, Politecnico di Milano, Milano, 2012.
29. Merritt HE. *Hydraulic control systems*. London: Wiley, 1967.
30. Bitz G. *Braking system with EBS and prefill function and electronic braking control method*. Patent 7806486, USA, 2010.
31. Freescale. *56F8300 hybrid controller used in control of electro-mechanical brake*. Application note, AN1999, 2004, http://www.freescale.com/files/dsp/doc/app_note/AN1999.pdf
32. Mare JC. Friction modelling and simulation at system level: a practical view for the designer. *Proc IMechE, Part I: J Systems and Control Engineering* 2012; 226(6): 728–741.
33. Canudas de Wit C, Olsson H, Astrom KJ, et al. A new model for control of systems with friction. *IEEE T Automat Contr* 1995; 40(3): 419–425.
34. Armstrong B, Dupont P, Canudas de and Wit C. A survey of models, analysis tools and compensation methods for the control of machines with friction. *Automatica* 1994; 30(7): 1083–1138.
35. Astrom J and Canudas-de Wit C. Revisiting the LuGre friction model. *IEEE Contr Syst Mag* 2008; 28(6): 101–114.
36. De Castro R, Araújo RE and Freitas D. Optimal linear parameterization for on-line estimation of tire-road friction. In: *18th world congress of the international federation of automatic control (IFAC)*, Milano, 28 August–2 September 2011, pp.8409–8414. International Federation of Automatic Control (IFAC).
37. Ziena Optimization Inc. KNITRO 6.0 user manual, March 2009.
38. Bin Y and Chang J. Advanced motion control: from classical PID to nonlinear adaptive robust control. In: *11th IEEE international workshop on advanced motion control*, Nagaoka, Japan, 21–24 March 2010, pp.815–829. New York: IEEE.
39. Khalil H. *Nonlinear systems*. 3rd ed.Upper Saddle River, NJ: Prentice Hall, 2002.
40. Ioannou PA and Sun J. *Robust adaptive control*. Upper Saddle River, NJ: Prentice Hall, 1996.
41. Farrell J and Polycarpou M. *Adaptive approximation based control: unifying neural, fuzzy and traditional adaptive approximation approaches*. Hoboken, New Jersey: John Wiley & Sons, 2006.